E-ISSN 2586-9027
Homepage : https://tci-thaijo.org/index.php/SciTechAsia Science & Technology Asia
Vol.30 No.3 July - September 2025 Page: [135-142]
Original research article

DNA Aptamer (LepDapt) Against Lipl32 as A Potential Diagnostic Agent for Detection of Leptospira

Tri Cao Vu[1], Boonchoy Soontornworajit[1,2], Yuthana Tantirungrotechai[1,2,*]

[1]*Division of Chemistry, Faculty of Science and Technology, Thammasat University, Pathum Thani 12120, Thailand*
[2]*Sirindhorn International Institute of Technology, Thammasat University, Pathum Thani 12120, Thailand*

Received 16 June 2025; Received in revised form 21 July 2025
Accepted 29 July 2025; Available online 30 September 2025

ABSTRACT

Leptospirosis is an infectious disease caused by pathogenic Leptospira spp. To enable early detection, DNA aptamers (LepDapt) were developed to target LipL32, the most abundant outer membrane protein in pathogenic Leptospira. Among the identified candidates, LepDapt-5a exhibited the strongest binding affinity. Molecular dynamics (MD) simulations show that LepDapt-5a forms a stable G-quadruplex (G4) structure. While the G-quadruplex serves as the primary contributor to LepDapt-5a's interaction with LipL32, the adjacent double helix enhances binding affinity by increasing the interaction surface. Analysis of per-residue binding energy via MM/PBSA highlights the significant roles of T19 and G24 in target interaction. To assess the impact of these residues, we used AlphaFold3 to predict the 3D structure of the DNA aptamers and docked them to LipL32 via HADDOCK2.4 webserver. MD simulations of all complexes were performed using the AMBER ff14SB and OL15 force fields for protein and nucleic acids, respectively. While the mutants preserved G4 formation, the G24 mutation disrupted the double helix structure but strengthened binding to LipL32. In contrast, mutation at T19 preserved the helical structure but weakened binding. The binding free energy (ΔG) of LepDapt-5a, computed via the MM/PBSA method, was estimated to be –12.45 ± 12.99 kcal/mol. This value is consistent with experimental data of dissociation constants (Kd) of 33.97 ± 5.30 nM.

Keywords: Aptamer engineering; Leptospirosis; LipL32 protein; MD simulations

***Corresponding author:** yuthana$_t$ *@tu.ac.th* **doi:** 10.14456/scitechasia.2025.56

1. Introduction

Leptospirosis is a tropical disease caused by Leptospira spp., typically transmitted through contact with contaminated water or soil. While most cases are mild, severe manifestations such as Weil's syndrome and severe pulmonary hemorrhage syndrome can be fatal, with mortality rates as high as 70% in the latter [1]. Early detection is critical, yet current diagnostic methods often lack sensitivity during early infection [2].

LipL32, the most abundant outer membrane protein found in pathogenic Leptospira spp., is surface-exposed, highly conserved across virulent strains, and has strong immunogenicity [3]. It is known to bind extracellular matrix components such as fibronectin, laminin, and collagens I, IV, and V; suggesting a role in host-pathogen interaction [4]. LipL32 has been widely used in serological diagnostics [3, 5] and vaccine research [6, 7]. These characteristics also make it an ideal target for aptamer-based molecular recognition. Aptamers, short single-stranded oligonucleotides, offer advantages over antibodies, including stability and specificity. To this end, Yeoh and co-workers developed a series of LipL32-binding aptamers, notably LepDapt-5a [8], though its structure and binding mechanism remain unclear.

This study investigates the structural dynamics of the LepDapt-5a aptamer, with a focus on its hypothesized G-quadruplex (G4) formation and its interaction with LipL32, using MD simulations, with Amber forcefields ff14SB and OL15 for protein and nucleic acids respectively.

2. Computational Methods

2.1 Lepdapt-5a structure predicted with alphafold3

Conventional 2D structure predictors such as mFold, RNAstructure, and ViennaRNA cannot model Hoogsteen base pairing. To address this limitation, we employed AlphaFold3 [9] to predict the structure of LepDapt-5a. The structure with the highest PLDDT score was selected.

2.2 Docking to LipL32

The predicted model was then docked to LipL32 (UniProt ID: O34094) using HADDOCK2.4 webserver [10] with default settings. The cluster with the lowest score was used for MD simulations.

2.3 Systems preparation

All systems were placed in dodecahedral simulation boxes. Each box was solvated using the TIP3P water model and neutralized with 0.15 M NaCl. Periodic boundary conditions were applied, with a 10 $\mathring{A}$ cutoff for non-bonded interactions. Bonds involving hydrogen atoms were constrained using the LINCS algorithm. The simulation protocol included: (a) 5000 steps of steepest descent energy minimization, (b) 500 ps of NVT equilibration to heat the system from 0 K to 300 K using V-rescale temperature coupling, (c) 500 ps of NPT equilibration at 300 K and 1 bar with harmonic restraints and C-rescale pressure coupling, and (d) 150 ns of production MD with 2.0 fs time step. The final 100 ns of each trajectory were analyzed using GROMACS 2023.2 [11] and visualized with ChimeraX version 1.9. [12]

2.4 Free energy calculation with MMPB/GBSA

Binding free energies were computed using gmx_MMPBSA v1.6.3 [13], applying MM/PBSA and MM/GBSA methods [14] with a single-trajectory approach. The following equations were used:

$$\Delta G_{blind} = \langle G_{COM} \rangle - \langle G_{REC} \rangle - \langle \Delta G_{LIG} \rangle, \quad (2.1)$$

$$\langle G_x \rangle = \langle E_{MM} \rangle + \langle G_{SOL} \rangle - \langle TS \rangle, \quad (2.2)$$

where $\langle G_{COM} \rangle$, $\langle G_{REC} \rangle$, $\langle \Delta G_{LIG} \rangle$ are defined in Eq. (2.2); $\langle E_{MM} \rangle$ corresponds to the molecular mechanical energy changes in the gas phase. $\langle G_{SOL} \rangle$ is the solvation free energy which can be divided into polar and non-polar contributions. $\langle TS \rangle$ is Entropy contribution.

3. Results and Discussion

3.1 Lepdapt-5a has a stable G-quadruplex structure

The root mean square deviation (RMSD) of unbound LepDapt-5a averaged 0.38 ± 0.09 nm, as shown in [Fig. 1(f)] and Table 1, indicating that the aptamer maintains a stable overall structure. The torsion angles of each tetrad [Fig. 1(d)] remained close to 06∘, and the inter-tetrad distances [Fig. 1(e)] were approximately 0.5 nm, further confirming the formation of a stable G4 structure, regardless of binding state, thereby supporting the hypothesis proposed by Yeoh et al.

Although AlphaFold3 represents a major advancement for protein-nucleic acids structural prediction. It still faces limitations due to a sparse and biased training set, which includes only approximately 7,800 RNA/DNA structures compared to over 216,000 protein structures [15]. This leads to incomplete modeling of key nucleic acid features such as non-Watson-Crick base paring, base stacking geometry [15]; ions- and pH- dependent folds behaviors [15, 16]; and DNA structural variations beyond the canonical B-form [9, 15, 17]. Nonetheless, AlphaFold3 demonstrates reasonable accuracy for nucleic acid sequences shorter than 300 nucleotides (nt), with a sharp drop in accuracy for sequences exceeding 500nt [18, 19]. In our study, the LepDapt-5a aptamer is relatively short, consisting of only 28 nt; therefore, we selected AlphaFold3 to predict its structure. However, the best recommended practice is to compare AlphaFold3 predictions with alternative structure predictors, followed by MD simulations for further validation, as we have done and shown in Fig. 1.

Table 1. The average RMSD of LepDapt-5a at bound and unbound states with LipL32.

Components	RMSD (nm) Bound	RMSD (nm) Unbound
Complex	0.37 ± 0.06	-
LipL32	0.30 ± 0.05	0.47 ± 0.10
LepDapt-5a	0.55 ± 0.11	0.38 ± 0.09
G-quadruplex	0.23 ± 0.04	0.36 ± 0.09
D-helix	0.63 ± 0.17	0.41 ± 0.10

Upon complex formation with LipL32, the protein exhibited increased structural stability, while LepDapt-5a showed a slight increase in flexibility, particularly in the D-helix region, where the RMSD increased from 0.41 ± 0.10 nm to 0.63 ± 0.17 nm. As shown in [Fig. 1(g)], the quadruplex structure is the main binding contributor toward LipL32 with key hydrogen bonding and electrostatic interactions were observed between DG1–ASP195, DG10–LYS202, DG11–LYS202, DG14–TYR217, DG18–ASN176, and DG24–ASN188. An average of 6.52 ± 1.83 intermolecular hydrogen bonds were maintained during the simulation, further supporting the stability of the LepDapt-5a–LipL32 complex. The computed binding

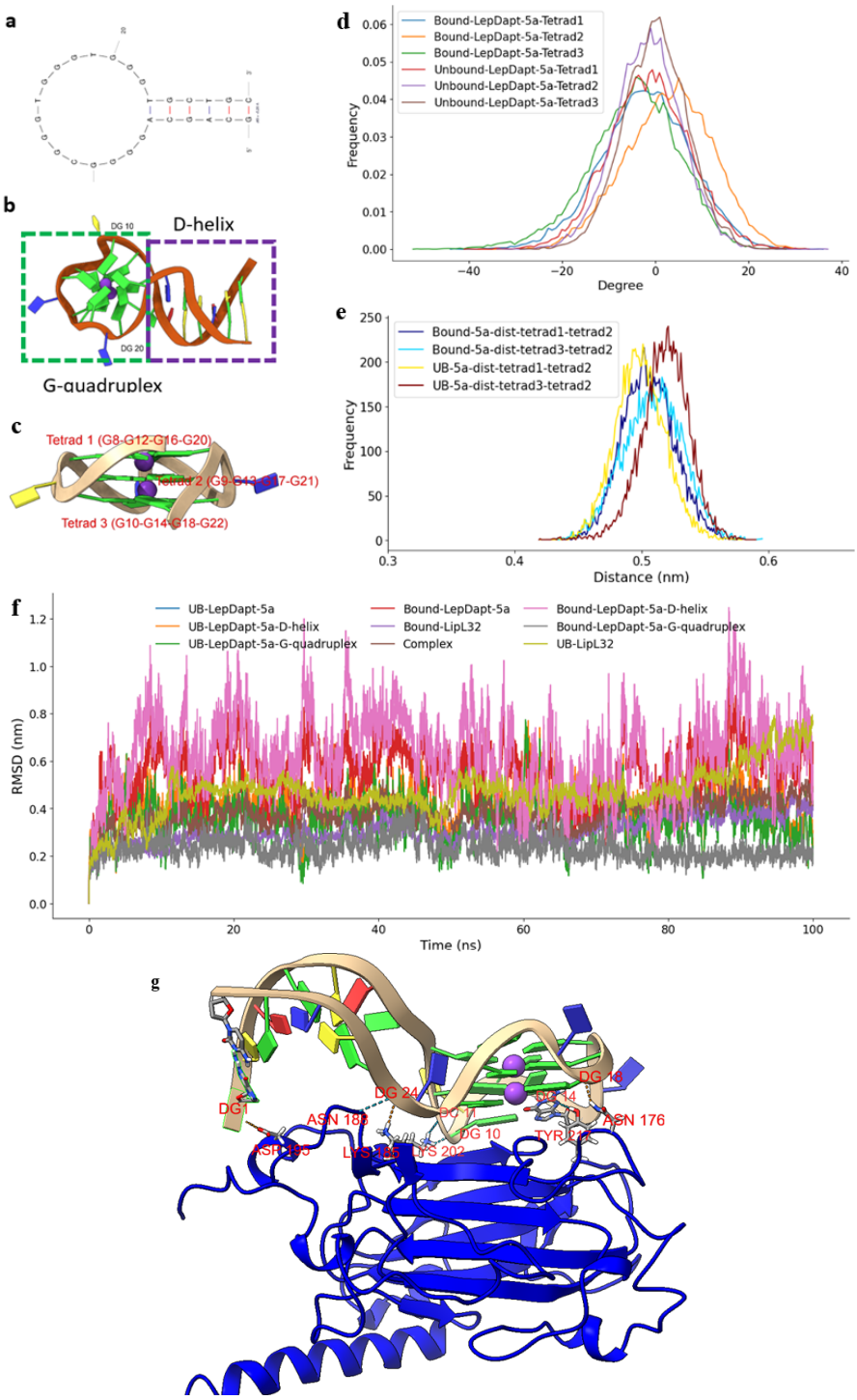

Fig. 1. LepDapt-5a structure (a) predicted by mFold. (b) predicted by AlphaFold3. (c) tetrad of G4 structure. (d) the torsion angle of each tetrad, (e) the inter-tetrad distances. (f) the RMSD of LepDapt-5a at bound and unbound (UB) states in respect to the structure at 50ns. (g) intermolecular H-bonds between LepDapt-5a and LipL32.

free energy via MM/PBSA was estimated to be –12.45 ± 12.99 kcal/mol, which agrees with the experimental dissociation constant (Kd) of 33.97 ± 5.30 nM [8].

3.2 Mutation on sequence on LepDapt-5a

The per-residue decomposed contribution of residues of LepDapt-5a (Table 2) revealed three categories of contribution: strong binding contributors (e.g., DT19: – 2.25 kcal/mol, DC25: – 1.12 kcal/mol, DG27: – 0.42 kcal/mol), strong anti-binding contributors (DG21: + 0.72 kcal/mol, DG22: + 1.30 kcal/mol, DG24: + 1.22 kcal/mol), and residues with minimal contribution ($|\Delta G| < 0.1$ kcal/mol). Based on this, we hypothesized that mutating residues with strong binding contributions (like DT19) would reduce binding affinity, while modifying residues with anti-binding effects (like DG24) could improve it. To preserve the core structural integrity, residues essential for G-quadruplex formation were not considered for mutation.

To test this hypothesis, we introduced single-point mutation at two representative positions: DT19 was mutated to its complementary base adenine (denoted as T19A), and DG24 to cytosine (G24C). These variants were selected to evaluate the structural and energetic consequences of altering residues with opposite binding roles.

3.3 Effects of T19C mutation

While the T19A mutation preserved the structure of LepDapt-5a, it led to overall destabilization of the aptamer, particularly in the D-helix region, which showed an increased RMSD of 0.79 ± 0.25 nm (Table 3). This mutation also reduced the interaction between LepDapt-5a and LipL32, leaving only the G4 core involved in binding (Fig. 2).

Table 2. The decomposed contribution of LepDapt-5a's residues to its binding affinity.

ID	Res-Name	Avg. (kcal/mol)
6	DA	-0.07
7	DG	-0.06
18	DG★	0.003
19	DT	-2.25
20	DG★	-0.05
21	DG★	0.72
22	DG★	1.30
23	DT	0.56
24	DG	1.22
25	DC	-1.12
26	DT	-0.06
27	DG	-0.42

Note: ★ residue that is crucial for G-quadruplex formation.

Table 3. RMSD of wild type, T19A, and G24C.

Components	WT	T19A	G24C
Complex	0.37 ± 0.06	0.38 ± 0.08	0.33 ± 0.06
LipL32	0.30 ± 0.05	0.32 ± 0.08	0.34 ± 0.07
LepDapt-5a	0.55 ± 0.11	0.55 ± 0.17	0.27 ± 0.05
G4	0.23 ± 0.04	0.20 ± 0.04	0.27 ±0.06
D-helix	0.63 ± 0.17	0.79 ± 0.25	-
Head	-	-	0.18 ± 0.04
Tail	-	-	0.34 ± 0.10

3.3.1 Effects of G24C mutation

The G24C mutation caused the D-helix of LepDapt-5a to break into distinct head and tail segments. This structural rearrangement increased the interaction surface and enabled the formation of new hydrogen bonds between both segments and LipL32, resulting in a decrease in RMSD across all components as shown in Table 3.

On average, 14.75 ± 1.92 intermolecular hydrogen bonds were maintained during the simulation, indicating improved interaction stability. However, the binding free energy computed via MM/PBSA was estimated to be 53.20 ± 21.02 kcal/mol, which unexpectedly indicates a reduction in binding affinity. This is likely due to increased entropic penalties arising from the flexible, fragmented D-helix. This discrepancy highlights a limitation of the MM/PBSA method, particularly in systems with high entropic contributions which

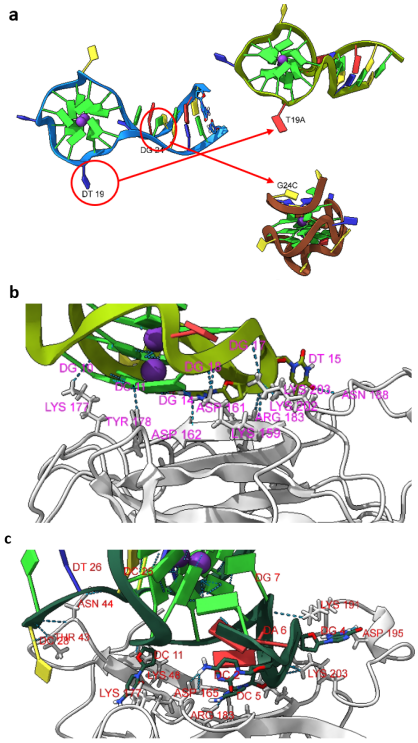

Fig. 2. (a) Structural comparison of T19A and G24C single-point mutations in LepDapt-5a. (b)-(c) Binding interface of the T19A mutant and G24C mutant.

will be explored in future studies using alchemical MD methods such as nonequilibrium approaches, free energy perturbation (FEP), and thermodynamics integration (TI). These methods evaluate the free energy change when the ligand is transformed from the original structure (state A) to its mutated structure (state B). The double-delta free energy difference ($\Delta\Delta G$) will indicate whether the mutation is energetically favorable.

4. Conclusion

This study provides computational evidence that LepDapt-5a forms a stable G-quadruplex structure, supporting prior experimental assumptions regarding its molecular conformation. The G-quadruplex serves as the primary recognition element for LipL32, while the adjacent D-helix enhances binding through additional surface interactions. Structural changes due to single-point mutations, although not disrupting the core G4 motif, significantly alter binding interfaces and flexibility. While this work provides mechanistic insights through molecular dynamics and free energy analysis, additional experimental validation such as structural or binding assays on the mutants would further strengthen these conclusions. Such studies are currently in progress and will be addressed in future publication. These findings offer a deeper understanding of aptamer-target interactions and support the development of LepDapt-5a as a potential diagnostic tool for leptospirosis.

Acknowledgements

Mr. Tri Cao Vu acknowledges the Scholarship for Research, Internationalization, and Education from Thammasat University, Academic Year 2566, for his M.Sc. study. This research is supported by Thailand Science Research and Innovation (TSRI) Fundamental Fund, fiscal year 2025.

References

[1] Lethal pulmonary hemorrhage syndrome due to Leptospira infection transmitted by pet rat. PubMed. Available from: https://pubmed.ncbi.nlm.nih.gov/28491815/. Accessed 2025 Jun 16.

[2] Behera SK, Sabarinath T, Ganesh B, Mishra PKK, Niloofa R, Senthilkumar K, et al. Diagnosis of Human Leptospirosis: Comparison of Microscopic Agglutination Test with Recombinant LigA/B Antigen-Based In-House IgM Dot ELISA Dipstick Test and Latex Agglutination Test Using Bayesian Latent Class Model

and MAT as Gold Standard. Diagnostics (Basel). 2022;12:1455.

[3] da Rosa MC, Martins G, Rocha BR, Correia L, Ferronato G, Lilenbaum W, et al. Assessment of the immunogenicity of the leptospiral LipL32, LigAni, and LigBrep recombinant proteins in the sheep model. Comp Immunol Microbiol Infect Dis. 2019;65:176–80.

[4] Hauk P, Barbosa AS, Ho PL, Farah CS. Calcium binding to leptospira outer membrane antigen LipL32 is not necessary for its interaction with plasma fibronectin, collagen type IV, and plasminogen. J Biol Chem. 2012;287:4826–34.

[5] Coutinho ML, Vasconcellos FA, Fernandes CPH, Seyffert N, Seixas FK, Ko AI, et al. Evaluation of the Anti□LipL32 Monoclonal Antibodies Potential for Use in Leptospirosis Immunodiagnostic Tests. J Immunoassay Immunochem. 2007;28:279–88.

[6] Di Azevedo MIN, Borges ALDSB, Kremer F, de Melo JDSL, Carvalho-Costa FA, Lilenbaum W. Genetic Analysis of LigA, LipL32, Loa22, and OmpL1 Antigens from Leptospira spp. Sejroe Serogroup: How Close We Are To a Vaccine Against Bovine Leptospirosis? Curr Microbiol. 2023;80:310.

[7] Samakchan N, Thinwang P, Boonyom R. Oral immunization of rat with chromosomal expression LipL32 in attenuated Salmonella vaccine induces immune respond against pathogenic Leptospira. Clin Exp Vaccine Res. 2021;10:217–28.

[8] Yeoh TS, Tang T-H, Citartan M. Isolation of a novel DNA aptamer against LipL32 as a potential diagnostic agent for the detection of pathogenic Leptospira. Biotechnol J. 2023;18.

[9] Accurate structure prediction of biomolecular interactions with AlphaFold 3. Nature. Available from: https://www.nature.com/articles/s41586-024-07487-w. Accessed 2024 Aug 2.

[10] Honorato RV, Trellet ME, Jiménez-García B, Schaarschmidt JJ, Giulini M, Reys V, et al. The HADDOCK2.4 web server for integrative modeling of biomolecular complexes. Nat Protoc. 2024.

[11] GROMACS: High performance molecular simulations through multi-level parallelism from laptops to supercomputers. ScienceDirect. Available from: https://www.sciencedirect.com/science/article/pii/S2 Accessed 2024 May 7.

[12] Pettersen EF, Goddard TD, Huang CC, Meng EC, Couch GS, Croll TI, et al. UCSF ChimeraX: Structure visualization for researchers, educators, and developers. Protein Sci. 2021;30:70–82.

[13] Valdés-Tresanco MS, Valdés-Tresanco ME, Valiente PA, Moreno E. gmx_MMPBSA: A New Tool to Perform End-State Free Energy Calculations with GROMACS. J Chem Theory Comput. 2021;17:6281–91.

[14] Miller BRI, McGee TDJr, Swails JM, Homeyer N, Gohlke H, Roitberg AE. MMPBSA.py: An Efficient Program for End-State Free Energy Calculations. J Chem Theory Comput. 2012;8:3314–21.

[15] Bernard C, Postic G, Ghannay S, Tahi F. Has AlphaFold3 achieved success for RNA? Acta Crystallogr D Struct Biol. 2025;81:49–62.

[16] Abramson J, Adler J, Dunger J, Evans R, Green T, Pritzel A, et al. Accurate structure prediction of biomolecular interactions with AlphaFold 3. Nature. 2024;630:493–500.

[17] Ochoa S, Milam VT. Direct Modeling of DNA and RNA Aptamers with AlphaFold 3: A Promising Tool for Predicting Aptamer Structures and Aptamer–Target Interactions. ACS Synth Biol. 2025.

[18] Krokidis MG, Koumadorakis DE, Lazaros K, Ivantsik O, Exarchos TP, Vrahatis AG, et al. AlphaFold3: An Overview of Applications and Performance Insights. Int J Mol Sci. 2025;26:3671.

[19] Xu S, Feng Q, Qiao L, Wu H, Shen T, Cheng Y, et al. FoldBench: An All-atom Benchmark for Biomolecular Structure Prediction. 2025 May 22.